# Low-$Q^2$ nucleon structure from an infrared-saturated evolution scheme

Rong Wang (王荣)[1,2,3†]

[1]Institute of Modern Physics, Chinese Academy of Sciences, Lanzhou 730000, China
[2]School of Nuclear Science and Technology, University of Chinese Academy of Sciences, Beijing 100049, China
[3]Advanced Energy Science and Technology Guangdong Laboratory, Huizhou 516007, China

**Abstract:** The low-$Q^2$ nucleon structure is described using a simple nonperturbative input of three valence quarks and an all-order infrared-saturated evolution scheme, showing consistency with experimental data. The resonance peaks in the experimental data for the $F_2$ structure function are found to be modulated by the valence quark distributions. Due to the small sea quark distributions at low $Q^2$, the valence-quark bump is clearly visible in the structure function. The three valence quark distributions at the hadronic scale are found to be the dominant contribution to the PDFs at hard scales. High-twist corrections are needed to explain the significant discrepancy between theory and experimental measurements at low $Q^2$. The infrared-saturated evolution scheme is a powerful tool for connecting nucleon structure in the nonperturbative and perturbative regions.

**Keywords:** nucleon structure, DGLAP evolution equations, quark model, low-Q2 structure function

**DOI:** **CSTR:**

CPC Accepted

## I. INTRODUCTION

Mapping the nucleon structure precisely is a central topic in particle and nuclear physics, as it is closely related to intricate and puzzling nonperturbative phenomena, such as emergent hadron mass [1−6] and color confinement [7−11]. With the forthcoming Electron-Ion Collider (EIC) [12, 13], the proposed Electron-ion collider in China (EicC) [14−17] and the JLab 24 GeV upgrade [18], the nucleon structure will be measured with much greater precision over a broad kinematic region, providing multi-dimensional information to finally tackle the challenging issues of the strong interaction in the nonperturbative regime. The study of nucleon structure is essential for a complete understanding of the complex dynamics of the strong interaction, which is described by quantum chromodynamics (QCD) [19−23].

The central objects for describing the nucleon structure are parton distribution functions (PDFs) $f(x)$ [24−27], defined as the number density of partons carrying a fraction $x$ of the longitudinal momentum of the nucleon in the infinite-momentum frame (or on the light cone). The precise determination of PDFs from global analyses [28−31] has been a remarkable milestone for QCD theory. Yet, the origin of PDFs and the infrared evolution of the nucleon structure remain unresolved. The nucleon structure can be evaluated efficiently at low $Q^2$, because the sea quark and gluon degrees of freedom are frozen. However, a comprehensive understanding of how to link the calculations in the infrared region to the experimental measurements at high scales is still lacking.

Nonperturbative effects must be incorporated into the PDF evolution with the $Q^2$ scale in the low-$Q^2$ domain. Recently, an infrared-saturated evolution scheme has been proposed to soundly extend QCD evolution to $Q^2 \approx 0$ GeV$^2$ [32], incorporating effective parton mass, a saturating running strong coupling, and parton-parton recombination. This evolution scheme is also argued to be all-order exact [33]. In this scheme, a saturating running coupling of the effective QCD charge and leading-order parton splitting kernels are used. Because all higher-order corrections are absorbed into the definition of the effective QCD charge [33], the scheme is referred to as all-order exact. Such an infrared-saturated evolution scheme can be regarded as a useful model for PDF evolution at low $Q^2$. With this novel evolution scheme, PDFs can be evolved consistently over the entire $Q^2$ range from 0 GeV$^2$ to infinity.

With the help of this new evolution scheme, we first investigate the origin of PDFs. According to the naive quark model, the nucleon consists of three quarks, the minimal number required to form a color singlet. Without the contributions of sea quark and gluon distributions, the valence quark distribution should manifest as a bump in the structure function at extremely low $Q^2$. Second, it is important to test nonperturbative model calculations. For example, the valence quark distributions estimated in the infrared region from the maximum entropy method [34]

Received 5 August 2026; Accepted 4 November 2026

† E-mail: rwang@impcas.ac.cn

©2027 Chinese Physical Society and the Institute of High Energy Physics of the Chinese Academy of Sciences and the Institute of Modern Physics of the Chinese Academy of Sciences and IOP Publishing Ltd. All rights, including for text and data mining, AI training, and similar technologies, are reserved.

are tested against the proposed infrared-saturated evolution equations. Third, we aim to demonstrate factorization violation [35−37], by comparing theoretical predictions with experimental measurements of the $F_2$ structure function at low $Q^2$ scales.

The idea of interpreting low-$Q^2$ nucleon structure in terms of three valence (constituent) quarks dates back to the early days of QCD [38−41]. At that time, limited DIS data with large uncertainties allowed the three-quark model to provide a reasonable fit. However, in the 1990s, more precise DIS data became available, and QCD analyses showed that substantial valence-like gluon distributions at low $Q^2$ were necessary to quantitatively describe structure functions measured at high $Q^2$ [42−44]. Alternatively, incorporating the substructure of constituent quarks could resolve discrepancies between DIS data and pure valence quark model predictions [45−47].

The validity of the pure valence quark picture at low $Q^2$ has also been examined via PDF positivity constraints at the hadronic scale and through the backward evolution of sea quark and gluon moments. In Ref. [48], a reliable method for solving Dokshitzer-Gribov-Lipatov-Altarelli-Parisi (DGLAP) evolution equations [49−51] across large scale separations was proposed, showing that PDF positivity requires $Q_0 > 580$ MeV. This lower bound exceeds the scale associated with the pure valence quark model, indicating that the pure valence interpretation of low-$Q^2$ nucleon structure is inconsistent with PDF positivity. Recent systematic studies of the backward evolution of Mellin moments for various PDF sets further show that sea quark and gluon distributions cannot be generated solely through perturbative QCD radiation [52]. For instance, the gluon Mellin moments at different moment indices $n$ do not vanish at a common $Q_0^2$ scale. Moreover, sea quark and gluon moments do not approach zero simultaneously around the same $Q_0^2$ scale. Using the HERAPDF (NNLO) set, one sea quark moment remains non-zero even when $\alpha_s$ is as large as 3, while the gluon distribution at small $x$ becomes significantly negative at such scales.

The low-$Q^2$ behavior of nucleon structure has been investigated using modified evolution equations that include threshold resummation effects at large $x$. Large logarithmic corrections arising from the threshold region can spoil perturbative expansions, necessitating the resummation of these corrections to all orders in $\alpha_s$ – a technique known as threshold resummation. This is implemented by shifting the renormalization scale from $Q^2$ to $Q^2(1-z)/z$ in the parton density evolution at large $x$. In Ref. [53], it was found that while this scale modification does not improve the description of DIS data, it obviates the need for a valence-like gluon distribution and yields a more natural gluon distribution at very low $Q^2$. The analysis also hints at a frozen $\alpha_s$ to account for higher-order corrections. In Ref. [54], a nonperturbative hadronic model is connected to perturbative QCD using modified evolution that includes target mass corrections and large-$x$ resummation. The study suggests a saturated running coupling in the infrared region under a novel effective charge definition [55]. In this work, we also address low-$Q^2$ nucleon structure via modified DGLAP evolution, incorporating further nonperturbative corrections. In addition to employing a saturated $\alpha_s$ in the infrared region, we introduce a massive parton propagator to freeze the DGLAP evolution at very low $Q^2$ and include parton-parton recombination corrections to suppress gluon splitting at small $x$.

The organization of the paper is as follows. The input valence quark distributions at the hadronic scale and the nonperturbative effects within the Continuum Schwinger Methods (CSMs) [6] are discussed in Sec. II. How the nonperturbative effects modify the evolution equations and the resulting infrared-saturated evolution equations are presented in Sec. III. The predicted $F_2$ structure functions at low $Q^2$ are shown and compared with JLab data [56] in Sec. IV. The discussions of the origin of PDFs and the factorization violation at low $Q^2$ are also provided in Sec. IV. A concise summary is provided in Sec. V.

## II. NONPERTURBATIVE EFFECTS

All the complex strong interaction dynamics at long distances are reflected in the nonperturbative input to PDFs. This input consists of the initial PDFs at the hadronic scale, defined as the scale at which the nucleon contains only valence quarks and the minimal necessary components, since the nonperturbative model lacks sea and gluon degrees of freedom. The nonperturbative input is related to the nucleon wave function at the low energy scale governed by the nonperturbative strong interaction.

Dynamical Chiral Symmetry Breaking (DCSB) is a prominent phenomenon in QCD [4, 57−64], which provides a mechanism for the dynamical generation of mass. In the chiral limit, a quark acquires a large mass through strong interactions with gluons at low momentum scales. Evaluations of the quark two-point Green function in both continuum Schwinger methods (CSMs) and Lattice QCD (LQCD) yield excellent and mutually consistent descriptions of the features of DCSB [62]. The large effective quark mass necessarily affects the splitting kernels of evolution equations, which are derived under the assumption of massless quarks. DCSB is an unavoidable nonperturbative effect in the infrared region.

To perform calculations in the infrared region, an infrared-finite strong coupling is needed. According to the recent definition of the QCD effective charge [65, 66], the running strong coupling saturates to a finite value in the infrared region, because the Landau pole is tamed by the dynamically generated gluon mass at low momentum.

CPC Accepted

This saturating $\alpha_s$ is an important ingredient of our calculations.

### A. Nonperturbative input of PDFs

Computing nucleon structure at an extremely low $Q^2$ scale is convenient because of the minimal number of constituents inside the nucleon at this scale. Nowadays, the nonperturbative input can be obtained from first-principles techniques, including continuum Schwinger methods (CSMs) [67−71] and lattice QCD simulations [72−77], as well as from many model calculations [34, 78−84]. For simplicity, this work uses the nonperturbative input from the maximum entropy method (MEM) [34]. The MEM valence quark distributions at low $Q^2$ are parameterized by a simple beta-function form, $Ax^B(1-x)^C$, and are explicitly written as,

$$\begin{aligned} xu_v(x,Q_0^2) &= 4.589x^{1.095}(1-x)^{1.000}, \\ xd_v(x,Q_0^2) &= 7.180x^{1.427}(1-x)^{2.456}. \end{aligned} \tag{1}$$

Fig. 1 shows the simplest nonperturbative input, consisting of just three valence quarks at an extremely low $Q^2$ scale, where only the valence components in the nucleon can be resolved or probed. The three valence quark distributions used as input are evaluated with MEM under the constraints of the quark model assumptions and the quark confinement radius [34]. This MEM nonperturbative input is found to be broadly consistent with global fits and experimental data [34].

### B. Dressed parton mass

The effective masses of quarks and gluons are important parameters that govern the modifications of the splitting kernels in QCD evolution equations in the infrared region. In the context of DCSB, the quark mass is a smooth function of momentum. The quark and gluon mass functions can be evaluated using Dyson-Schwinger equations, which take into account the contributions of an infinite set of diagrams [4, 85]. In practical calculations, a symmetry-preserving truncation of the diagrams (Rainbow-Ladder truncation) is applied [64, 86]. Nevertheless, Dyson-Schwinger equations predict a quark mass function that is in striking agreement with LQCD simulations.

Excellent fits to the dynamical mass functions $m_q(Q^2)$ of light quarks are provided by the following expression:

$$m_q(Q^2) = m_0 + \frac{m_1}{1+(Q^2/\sigma^2)^\lambda}. \tag{2}$$

The resulting fit parameters are summarized in Table 1 for the up-, down-, and strange-quark mass functions. The parametrization of the dynamical gluon mass function obtained from the Dyson-Schwinger equations is given by [4, 85].

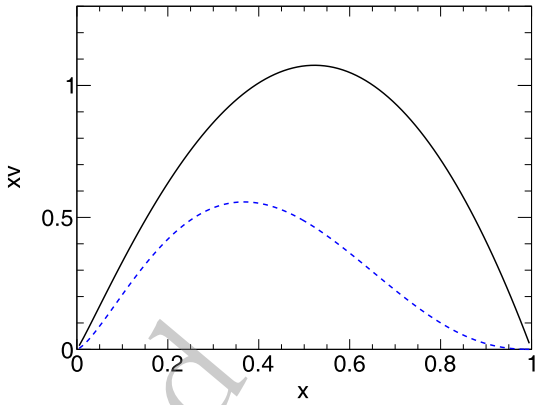



**Fig. 1.** (color online) The input parton distributions consist solely of valence quarks at the sufficiently low $Q_0^2$ scale. The solid and dashed curves show the up and down valence quark distributions, respectively.

**Table 1.** Fitted parameters for the dynamical mass functions of light quarks and the gluon obtained from numerical solutions of the Dyson-Schwinger equations (see Eqs. (2) and (3) for details).

| | $m_0$ [GeV] | $m_1$ [GeV] | $\sigma^2$ [GeV$^2$] | $\lambda$ |
|---|---|---|---|---|
| up / down | 0.002 | 0.394 | 0.625 | 1.51 |
| strange | 0.060 | 0.458 | 0.821 | 1.32 |
| | $m_0^4$ [GeV$^4$] | $\kappa_1^2$ [GeV$^2$] | $\kappa_2^2$ [GeV$^2$] | $\sigma^2$ [GeV$^2$] |
| gluon | 0.134 | 0.705 | 9.31 | 5.13 |

$$m_g^2(Q^2) = \frac{m_0^4}{\kappa_1^2 + Q^2\ln[(Q^2+\kappa_2^2)/\sigma^2]}. \tag{3}$$

The corresponding parameters are also presented in Table 1.

Figure 2 displays the dressed quark and gluon mass functions obtained from CSMs [4, 85]. The dressed quark mass decreases monotonically with increasing momentum. The constituent quark mass is smoothly connected to the current quark mass via the DCSB mechanism of complex strong interaction dynamics. In this work, the parametrized forms of these mass functions are employed in the subsequent calculations of the infrared-saturated evolution equations.

The dressed-parton mass differs significantly from the current or bare mass. It is the dynamical mass generated nonperturbatively in the Dyson-Schwinger equation framework through the resummation of infinitely many vacuum polarizations and related contributions [4, 85]. The dressed-parton propagator emerges as a consequence of long-range QCD screening, and the dynamical mass can be interpreted as the effective mass of a complex quasiparticle under this screening. The screening fields themselves are massless, but the complete vacuum polarization can acquire a mass scale at long distances. The gauge

CPC Accepted

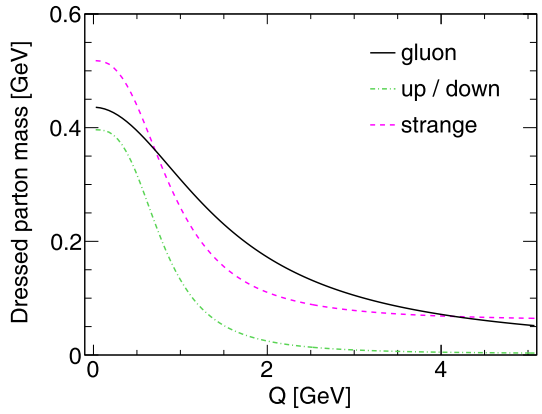



**Fig. 2.** (color online) The dressed parton mass as a function of momentum [4, 85]. The parton types are indicated in the figure.

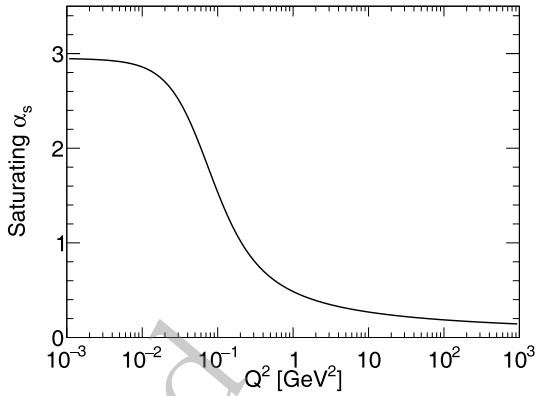



**Fig. 3.** The saturating running strong coupling $\alpha_s$ is shown as a function of the $Q^2$ scale [4, 65, 66, 71]. The running coupling saturates in the far-infrared region to around $\pi$.

boson can acquire a dynamical mass without violating gauge invariance. This effect serves as a key basis of the emergent hadron mass mechanism [4, 85].

### C. Saturating running strong coupling

The running strong coupling $\alpha_s$ is a key parameter in all QCD processes. To circumvent the divergence problem of the perturbative $\alpha_s$, we employ a renormalization-group-invariant and process-independent effective charge in QCD [4, 65, 66, 71]. Based on the concept of the QCD effective charge, the infrared behavior of $\alpha_s$ differs significantly from that of the traditional perturbative $\alpha_s$. The QCD effective charge yields a saturating $\alpha_s$ free from the Landau pole. At long distances, the screening effect is suppressed due to the large effective mass of the gluon. In this work, the saturating $\alpha_s$ is applied in the calculations of infrared-saturated evolution equations.

Figure 3 displays the saturating $\alpha_s$ obtained from CSMs [4, 65, 66, 71]. This effective charge provides an infrared completion with $\alpha_s/\pi \sim 0.97$ in the infrared limit. At high $Q^2$, it agrees well with the perturbative $\alpha_s$. Based on recent CSM calculations, a parametrization of the saturating $\alpha_s$ is given in Refs. [4, 65, 66, 71].

$$\alpha_s = \frac{\gamma_m \pi}{\ln[\mathscr{K}^2(k^2)/\Lambda_{\rm QCD}^2]},$$
$$\mathscr{K}(y) = \frac{a_0^2 + a_1 y + y^2}{b_0 + y}, \tag{4}$$

where $\gamma_m = 4/\beta_0$, $\beta_0 = 11 - (2/3)n_f$, and $\Lambda_{\rm QCD} = 0.234$ GeV.

## III. AN INFRARED-SATURATED EVOLUTION SCHEME

Considering the nonperturbative effects discussed above, we have proposed a novel infrared-saturated evolution scheme [32]. The parton mass suppresses parton radiation in DGLAP evolution [49–51] as $Q^2$ increases. The evolution speed is controlled by a factor $Q^2/(Q^2+M_q^2)$, where $M_q$ is the quark effective mass provided by DCSB. This factor originates from the $k_T$-dependent part of the splitting kernel with a massive propagator modification ($P_{qq}\frac{dk_T^2}{k_T^2+M_q^2} = P_{qq}\frac{d(k_T^2+M_q^2)}{k_T^2+M_q^2}$) and the corresponding transformation of the renormalization scale ($\frac{dxf}{d\ln(Q^2)} = \frac{Q^2}{Q^2+M^2}\frac{dxf}{d\ln(Q^2+M_q^2)}$) [32, 87]. The saturating $\alpha_s$ provides a finite interaction strength in QCD at any given momentum scale. The last ingredient of the infrared-saturated evolution scheme is the parton-parton recombination correction [88–90]. The parton-parton recombination process balances parton splitting, slowing the growth of the gluon distribution at small $x$ and ensuring that the cross-section unitarity is restored at high energy. Due to the large parton size at low $Q^2$, the parton-parton overlapping effect cannot be ignored at these scales.

By incorporating both nonperturbative effects and parton-parton overlapping, we obtain an infrared-saturated evolution scheme that is valid at any $Q^2$ scale. In this work, the infrared-saturated evolution scheme is applied to a MEM nonperturbative input to deliver nucleon PDFs at low $Q^2$ scales. The infrared-saturated evolution equations are written as,

$$\frac{dxq_{\rm i}^{\rm NS}}{d\ln(Q^2)} = \frac{Q^2}{Q^2+M_{\rm q}^2}\frac{\alpha_s(Q^2)}{2\pi}P_{\rm qq}\otimes xq_{\rm i}^{\rm NS}, \tag{5}$$

for the flavor non-singlet quark distributions,

$$\frac{dx\bar{q}_{\rm i}}{d\ln(Q^2)} = \frac{Q^2}{Q^2+M_{\rm q}^2}\frac{\alpha_s(Q^2)}{2\pi}\left[P_{\rm qq}\otimes x\bar{q}_{\rm i} + P_{\rm qg}\otimes xg\right]$$

CPC Accepted

$$-\frac{Q^2}{Q^2+M_{\rm q}^2}\frac{\alpha_{\rm s}^2(Q^2)}{4\pi R^2Q^2}\int_x^{1/2}\frac{dy}{y}xP_{{\rm gg}\to\bar{\rm q}}(x,y)[yg(y,Q^2)]^2 + \frac{Q^2}{Q^2+M_{\rm q}^2}\frac{\alpha_{\rm s}^2(Q^2)}{4\pi R^2Q^2}\int_{x/2}^{x}\frac{dy}{y}xP_{{\rm gg}\to\bar{\rm q}}(x,y)[yg(y,Q^2)]^2, \quad (6)$$

for the sea quark distributions, and

$$\frac{dxg}{d\ln(Q^2)} = \frac{Q^2}{Q^2+M_{\rm g}^2}\frac{\alpha_{\rm s}(Q^2)}{2\pi}\left[P_{\rm gq}\otimes x\Sigma + P_{\rm gg}\otimes xg\right] - \frac{Q^2}{Q^2+M_{\rm g}^2}\frac{\alpha_{\rm s}^2(Q^2)}{4\pi R^2Q^2}\int_x^{1/2}\frac{dy}{y}xP_{{\rm gg}\to{\rm g}}(x,y)[yg(y,Q^2)]^2 + \frac{Q^2}{Q^2+M_{\rm g}^2}\frac{\alpha_{\rm s}^2(Q^2)}{4\pi R^2Q^2}\int_{x/2}^{x}\frac{dy}{y}xP_{{\rm gg}\to{\rm g}}(x,y)[yg(y,Q^2)]^2, \quad (7)$$

for the gluon distribution, where $P_{\rm qq}$, $P_{\rm qg}$, $P_{\rm gg}$, $P_{\rm gq}$ are the standard splitting kernels, and $P_{{\rm gg}\to\bar{\rm q}}$, $P_{{\rm gg}\to{\rm g}}$ are the gluon-gluon recombination kernels. The factor $1/(4\pi R^2)$ in the equations serves as the two-parton density normalization; $R$ is the correlation length of two overlapping partons, as determined in a previous study [31]. The simplified parton-parton recombination correction, which includes only gluon-gluon recombination, is incorporated into the above DGLAP equations for computational efficiency. Although the parton-parton recombination processes $qg\to q(g)$, $qq\to q(q)$, and $q\bar{q}\to g(g)$ also exist, they are overwhelmed by the gluon-gluon recombination process [91]. Thus, the simplified parton-parton recombination correction yields almost the same results as the complete treatment. The evolution equations including the complete parton-parton recombination corrections can be found in Refs. [91, 92].

In the above equations, the factor $Q^2/(Q^2+M_{\rm q/g}^2)$ quenches the evolution at low $Q^2$, where $M_{\rm q/g}(Q^2)$ denote the mass functions obtained from CSMs. This factor originates from modifications to the standard evolution kernels (the splitting and recombination processes). Since $Q^2/(Q^2+M_{\rm q/g}^2)$ is independent of $x$, we factor it out of the integrals on the right-hand sides. The coupling $\alpha_{\rm s}(Q^2)$ is the saturating $\alpha_{\rm s}$ given in Eq. (4); it remains finite at all $Q^2$ scales. The terms containing $\int_x^{1/2}$ arise from the gluon-gluon recombination processes, which reduce the growth of parton density. The terms with $\int_{x/2}^{x}$ are anti-shadowing contributions that preserve momentum conservation in the gluon-gluon recombination processes.

## IV. RESULTS AND DISCUSSIONS

One prominent feature of the infrared-saturated evolution scheme is the freezing of PDF evolution as $Q^2$ approaches zero, explicitly indicated by the factor $Q^2/(Q^2+M_{\rm q/g}^2)$. It is found that the evolved PDFs are not sensitive to the choice of input hadronic scale $Q_0^2$, so long as $Q_0^2\lesssim 0.1$ GeV$^2$. Owing to the freezing of PDF evolution in the region $Q^2\approx 0$ GeV$^2$, a naive and natural choice of the hadronic scale is $Q_0^2=0$ GeV$^2$. In the following calculations, we set $Q_0^2=0.0001$ GeV$^2$ to enable rapid evolution of PDFs to a high $Q^2$ scale.

The infrared-saturated evolution equation is applied to the three valence quark distributions from MEM at $Q_0^2=0.0001$ GeV$^2$ to obtain the PDFs at higher $Q^2$. With the evolved PDFs, the proton structure functions are then computed at different $Q^2$ scales and shown in Fig. 4. One sees that the structure function peaks in the valence region at low $Q^2$ scales, owing to the tiny sea quark distribution at low scales. Thus, the valence-quark bump in the $F_2$ structure function at low $Q^2$ is strong proof that the dominant valence quark distributions are the origin of the PDFs measured at hard scales. In other words, the quark model description of the nucleon is the origin of the asymptotic partons in the infinite momentum frame.

In this work, the structure function $F_2$ is evaluated at leading order using evolved PDFs at high $Q^2$, since we apply the infrared-saturated evolution scheme that is all-order exact. In our calculations below, the leading-twist PDFs are provided and compared with the JLab data, which are defined as,

$$F_2=\sum_i e_{q_i}^2 x(q_i+\bar{q}_i), \quad (8)$$

in which $q_i$ denotes the quark distribution of flavor $i$, and $e_{q_i}$ denotes the corresponding electric charge of the quark. In a rigorous theoretical framework, the higher-twist contributions should not be ignored at low $Q^2$. Thus, the complete formula for the structure function $F_2$ is given by

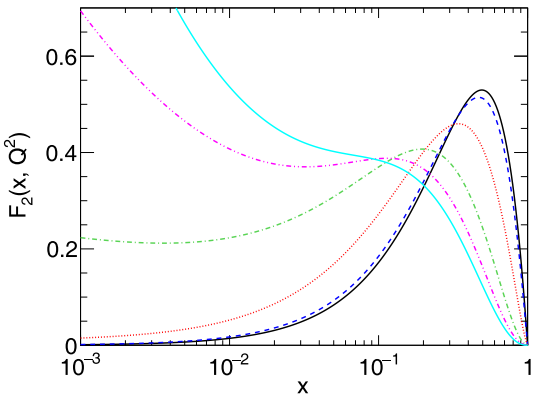



**Fig. 4.** (color online) The $F_2$ structure function obtained from the infrared-saturated evolution equation as a function of $x$ for different $Q^2$ scales: 0.001 GeV$^2$ (solid), 0.01 GeV$^2$ (dashed), 0.1 GeV$^2$ (dotted), 1 GeV$^2$ (dashed-dotted), 10 GeV$^2$ (dashed-dotted-dotted), and 100 GeV$^2$ (dashed-dotted-dotted-dotted).

CPC Accepted

$$F_2 = \sum_i e_{q_i}^2 x(q_i + \bar{q}_i) + \left( \sim \sum_n \frac{1}{Q^{2n}} \right)_{\text{high-twist}} . \quad (9)$$

As we lack a reliable model for higher-twist corrections in the non-perturbative region, we compute the structure function using only the leading-twist part (Eq. (8)). This is likely the primary reason for the factorization breakdown at low $Q^2$ shown below.

Our predicted structure functions are compared with the JLab measurement [56] at low $Q^2$ and large $x$, as shown in Fig. 5. At finite $Q^2$, the target-mass effect modifies the identification of the Bjorken variable $x$ with the light-cone momentum fraction. It has been argued that the finite target-mass effect can be removed by analyzing the structure functions in terms of the Nachtmann variable [93, 94], defined as $\xi = 2x/[1+\sqrt{1+4x^2M_N^2/Q^2}]$, where $M_N$ is the nucleon mass. At high $Q^2$, $\xi$ and $x$ are nearly identical. Therefore, we present the measured structure function at low $Q^2$ as a function of $\xi$. In Fig. 5, one finds that the experimental data are clearly lower than the theoretical predictions. However, the resonance peaks in the data are remarkably well described by our theoretical predictions. This indicates that quark-hadron duality holds at low $Q^2$ and that our theoretical calculations are broadly consistent with the experimental data.

Judging from the JLab data at different low $Q^2$ [56], one clearly sees the valence-quark bump in the measured structure function, regardless of the fluctuations caused by the resonances. The heights of the resonance peaks are well described by the dominant valence-quark distribution in the low-$Q^2$ region. According to quark-hadron duality, the experimental data at low $Q^2$ can be roughly interpreted in terms of the three valence-quark distributions. In conclusion, the quark-model description in the infrared region provides the dominant origin of the asymptotic partons observed at high energies.

In fact, we could adjust the three input valence-quark distributions to explain the low-$Q^2$ data slightly better. Nonetheless, the inherent inconsistency cannot be removed merely by tuning the non-perturbative input at $Q_0^2$. Moreover, the lower $Q^2$, the larger the discrepancy between theory and data. Our theoretical calculations are based on the factorization theorem. Therefore, we conclude that the lower $Q^2$, the more significant the factorization violation becomes. This finding is not surprising, since at low $Q^2$ sizeable higher-twist corrections are not included in the factorization formula. To improve the interpretation of low-$Q^2$ data, a study of higher-twist contributions is essential.

In line with earlier low-$Q^2$ studies using modified evolution equations [53, 54], we also find that an infrared-saturated strong coupling is necessary to smoothly connect the hadronic model with high-$Q^2$ experimental

CPC Accepted

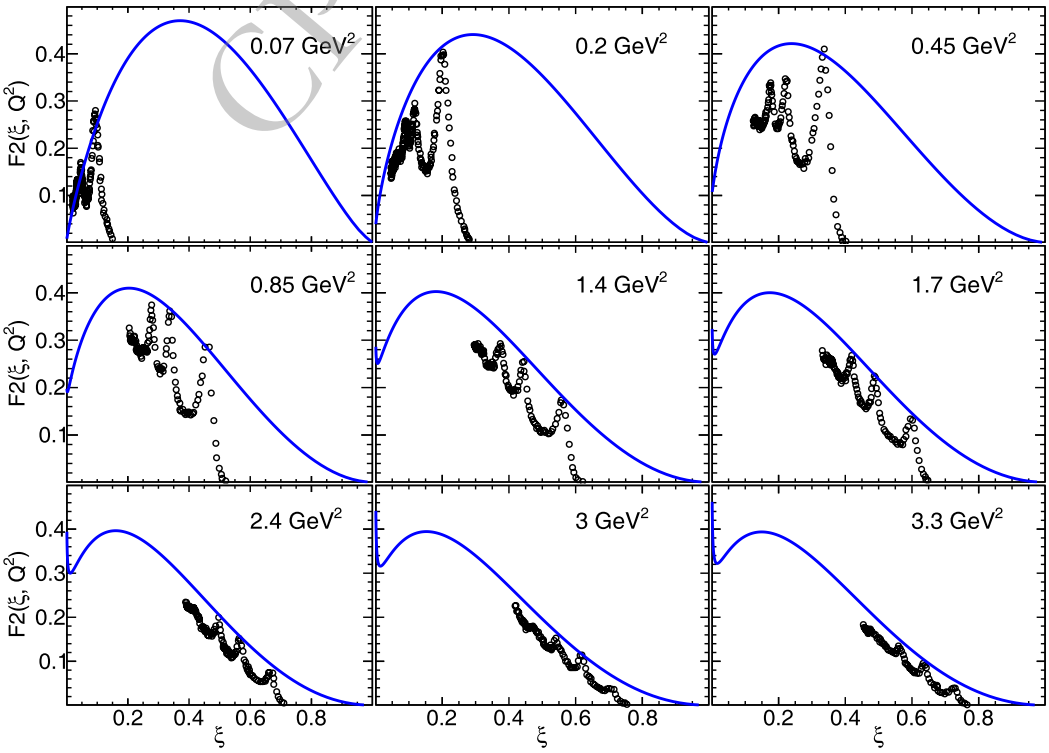



**Fig. 5.** (color online) The $F_2$ structure function is shown as a function of the Nachtmann variable $\xi$ at low $Q^2$ scales in the large-$x$ region. The circles represent the experimental data from JLab [56]. The curves show the predictions of the infrared-saturated evolution scheme.

data. Our analysis incorporates target-mass correction, the freezing of splitting functions during evolution, and parton–parton recombination effects, but not large-$x$ resummation, as we employ a leading-order DGLAP evolution framework. A recent analysis by the JAM collaboration shows that different computational methods for threshold resummation (Mellin-Fourier and double Mellin) lead to considerable differences in valence-quark distributions at large $x$ [95]. Based on the estimates [96–99], threshold resummation alone cannot resolve the significant discrepancy between our quark-model predictions and the structure function data at low $Q^2$.

Although our analysis shows that the resonance peaks in the $F_2$ data at low $Q^2$ are roughly modulated by the valence-quark distributions from the quark model, significant discrepancies remain, particularly when $Q^2$ falls below 0.5 GeV$^2$. Higher-twist effects are generally important at large $x$ and low $Q^2$. An earlier higher-twist analysis demonstrated that including data in the resonance region yields larger higher-twist coefficients, and that the $1/Q^4$ term also plays a significant role [100]. Similarly, higher-twist contributions were found to be crucial for accommodating the approximate scaling behavior of the proton Dirac form factor at intermediate $Q^2$ ($< 10$ GeV$^2$), in a recent study based on perturbative QCD $k_T$ factorization [101]. A later study by Courtoy and Liuti showed that the higher-twist effect could be absorbed into the strong coupling's infrared behavior, regulated by large-$x$ resummation [54]. A dedicated review of Bloom-Gilman (BG) duality in light of various experimental measurements suggests that the higher-twist contribution to the unpolarized $F_2$ structure function is only about 10–15% at $Q^2 \sim 1$–$2$ GeV$^2$ [102]. Interference among resonances leads to cancellations that suppress higher-twist contributions in integrated observables. BG duality holds because resonances – despite being built from infinite towers of higher twists – average to a leading-twist scattering behavior. The authors also argue that BG duality breaks down at very low $Q^2$, and for $Q^2 < 0.5$ GeV$^2$, twist-6 and higher terms become substantial [102]. Our results align with these previous findings.

The isoscalar structure function $xF_3$ is also provided using the valence quark distributions obtained from the infrared-saturated evolution equations. The $xF_3$ structure function is evaluated at leading twist in the form of leading order, as

$$xF_3(x,Q^2) = xu_v(x,Q^2) + xd_v(x,Q^2). \tag{10}$$

Fig. 6 compares the predicted $xF_3$ with experimental data from the CCFR [103] and NuTeV [104] collaborations. Contrary to our expectation, the predicted $xF_3$ at high $Q^2$ deviates significantly across the entire valence quark region, with the maximum relative deviation

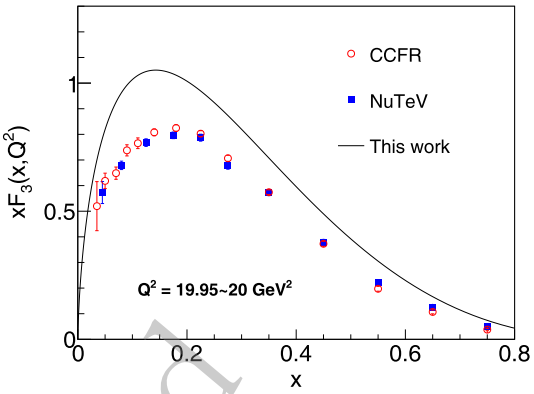



**Fig. 6.** (color online) The predicted $xF_3$ structure function, obtained from the nonperturbative input of MEM valence distributions and infrared-saturated evolution equations, is compared with experimental measurements by the CCFR (red circle, at 20 GeV$^2$) and NuTeV (blue square, at 19.95 GeV$^2$) collaborations.

slightly exceeding 20%. Several possible explanations for this discrepancy in our model calculations can be investigated in future studies. First, the input valence distributions at $Q_0^2$ from the MEM approach may not provide an accurate description of the nonperturbative input. Second, significant intrinsic sea quark components may be present at the input scale, necessitating a picture beyond the naive three-quark model at low resolution. Finally, the nuclear-medium correction used to extract the nucleon $xF_3$ data may be probe dependent [103, 104]. The structure function $xF_3$ is measured via neutrino and antineutrino deep-inelastic scattering on an iron target. Nuclear-target corrections are required to extract nucleon structure information. However, current data analyses adopt the nuclear-target correction derived from charged-lepton scattering measurements. This correction should be updated if nuclear effects are probe dependent.

## V. SUMMARY AND OUTLOOK

An infrared-saturated evolution scheme is applied to the initial three valence quark distributions at $Q_0^2$, in order to study the origin of PDFs. The three valence quarks of the quark model are found to be the dominant origin of the PDFs observed at hard scales. Irrespective of the resonance structures in the data, the JLab experiment has shown a clear valence-distribution bump in the measured $F_2$ structure function at low $Q^2$ scales. Quark-hadron duality is also observed.

The infrared-saturated evolution scheme serves as an essential bridge connecting the nucleon structure in the nonperturbative and perturbative regions. The dressed quark mass, the saturating $\alpha_s$, and the parton-parton overlap corrections are crucial for the validity and success of the infrared-saturated evolution scheme. Using this scheme, the quark model is smoothly linked to the parton

CPC Accepted

model, and the nucleon PDFs can be delivered over the entire momentum range from 0 $\mathrm{GeV}^2$ up to any desired high scale.

The quantitative study of high-twist phenomena is expected to improve the theoretical description of low-$Q^2$ data. By subtracting the leading-twist contribution to the structure function based on the PDFs, one can extract valuable information on the high-twist corrections at low $Q^2$ scales.

The quark model is quite successful in hadron classification (the mass spectroscopy at $Q^2 = 0$ $\mathrm{GeV}^2$). However, at such a low scale, quarks and gluons are completely frozen and do not act as dynamical degrees of freedom. As revealed in this work, the PDFs are almost completely frozen below 0.01 $\mathrm{GeV}^2$. The input of three valence quarks in this work is closely related to the three constituent quarks of hadron spectroscopy. Remarkably, the quark-model picture is partially demonstrated by the valence bump in the JLab $F_2$ data at extremely low $Q^2$. Due to the violation of factorization, the PDF at low $Q^2$ cannot be directly compared with the experimental data at low $Q^2$. Only the shape of the structure function resembles the valence distribution. In modern QCD, sea quarks and gluons constitute a small part of the nucleon's nonperturbative wave function. Indeed, some intrinsic strange and charm quarks are present in the nucleon at low $Q^2$. Nevertheless, these sea quarks and gluons carry only a small momentum fraction in the nucleon at low $Q^2$. Sea quarks and gluons are predominantly of perturbative origin. Overall, this work finds that the nonperturbative input of three valence quarks is too simplistic to accurately describe the experimental data. The nucleon structure is much richer than the simple quark-model picture implies.

The theoretical framework of infrared-finite evolution equations with a saturating strong coupling used in this work should be regarded as an effective model rather than as conventional perturbative QCD predictions. The saturating running strong coupling derived from the QCD effective charge is adopted in this study; it should be viewed as an effective coupling, not the leading-order coupling of perturbative QCD. As argued in Ref. [33], the QCD effective charge is defined through a formula in which the chosen observable is expressed solely in terms of the first-order perturbative coupling. Thus, by definition, the effective charge implicitly incorporates terms of arbitrarily high order in the perturbative coupling [33], making it an all-order effective description for low-$Q^2$ physics. This is why the formulas for the evolution equations and experimental observables are all expressed in the form of leading-order perturbative QCD. The QCD effective charge can be process dependent and is usually defined via the Bjorken sum rule [105]. For a given observable, it is renormalization-scheme independent by construction and remains finite everywhere, including in the infrared limit. We emphasize that the proposed infrared-saturated evolution scheme should be applied as an effective model for low-$Q^2$ physics, rather than as a rigorous perturbative QCD theory. All parameters in the model are fixed except for the input parton distributions at the hadronic scale, which can be tested and optimized in the future with more experimental data.

At very low $Q^2$, the factorization framework is not valid, and high-twist terms are expected to be significant. Thus, the model predictions at low $Q^2$ in this work cannot be compared directly and precisely to experiment unless rigorous modifications to factorization are made. The proposed infrared-saturated evolution scheme should be regarded only as an efficient model for connecting the nucleon structure at extremely low $Q^2$ to experimental measurements at high $Q^2$, as it has not yet been rigorously justified in nonperturbative QCD theory.

The low-$Q^2$ nucleon structure presented in this work and the high-twist QCD corrections can be further studied and tested at future high-energy facilities, such as the EIC [12, 13], EicC [14−17], and the JLab 24 GeV program [18]. To access the low-$Q^2$ data, electrons scattered at very small angles must be efficiently detected. Given the difficulty in detecting small-angle electrons, the low-energy EicC is somewhat more suitable for accessing low-$Q^2$ nucleon structure data. More high-precision experimental data are anticipated to finally resolve the problems concerning the transition from the nonperturbative to the perturbative region.

CPC Accepted

## ACKNOWLEDGMENTS

*The author gratefully acknowledges the insightful discussions with Professors Craig D. Roberts and Wei Zhu on the saturation of the strong coupling in the nonperturbative regime, DGLAP evolution equations, and parton-parton recombination processes.*

## References

[1] M. Ding, C. D. Roberts, and S. M. Schmidt, Particles **6**, 57 (2023), arXiv: 2211.07763[hep-ph]

[2] J. Papavassiliou, Chin. Phys. C **46**, 112001 (2022), arXiv: 2207.04977[hep-ph]

[3] D. Binosi, Few Body Syst. **63**, 42 (2022), arXiv: 2203.00942[hep-ph]

[4] C. D. Roberts, D. G. Richards, T. Horn, and L. Chang, Prog. Part. Nucl. Phys. **120**, 103883 (2021), arXiv: 2102.01765[hep-ph]

[5] D. S. Carman, R. W. Gothe, V. I. Mokeev, and C. D. Roberts, Particles **6**, 416 (2023), arXiv: 2301.07777[hep-ph]

[6] C. D. Roberts and A. G. Williams, Prog. Part. Nucl. Phys. **33**, 477 (1994), arXiv: hep-ph/9403224
[7] K. G. Wilson, Phys. Rev. D **10**, 2445 (1974)
[8] M. Bander, Phys. Rept. **75**, 205 (1981)
[9] G. 't Hooft, Nucl. Phys. B **190**, 455 (1981)
[10] A. M. Polyakov, Nucl. Phys. B **120**, 429 (1977)
[11] S. Mandelstam, Phys. Rept. **23**, 245 (1976)
[12] R. Abdul Khalek *et al*., Nucl. Phys. A **1026**, 122447 (2022), arXiv: 2103.05419[physics.ins-det]
[13] A. Accardi *et al*., Eur. Phys. J. A **52**, 268 (2016), arXiv: 1212.1701[nucl-ex]
[14] X. Chen, PoS **DIS2018**, 170 (2018), arXiv: 1809.00448[nucl-ex]
[15] X. Chen, F.-K. Guo, C. D. Roberts, and R. Wang, Few Body Syst. **61**, 43 (2020), arXiv: 2008.00102[hep-ph]
[16] D. P. Anderle *et al*., Front. Phys. (Beijing) **16**, 64701 (2021), arXiv: 2102.09222[nucl-ex]
[17] R. Wang and X. Chen, Few Body Syst. **63**, 48 (2022)
[18] A. Accardi *et al*., Eur. Phys. J. A **60**, 173 (2024), arXiv: 2306.09360[nucl-ex]
[19] D. J. Gross and F. Wilczek, Phys. Rev. Lett. **30**, 1343 (1973)
[20] H. D. Politzer, Phys. Rev. Lett. **30**, 1346 (1973)
[21] C.-N. Yang and R. L. Mills, Phys. Rev. **96**, 191 (1954)
[22] H. Fritzsch, M. Gell-Mann, and H. Leutwyler, Phys. Lett. B **47**, 365 (1973)
[23] G. 't Hooft and M. J. G. Veltman, Nucl. Phys. B **44**, 189 (1972)
[24] R. L. Workman *et al*. (Particle Data Group), PTEP **2022**, 083C01 (2022)
[25] J. D. Bjorken, Phys. Rev. **179**, 1547 (1969)
[26] R. P. Feynman, Phys. Rev. Lett. **23**, 1415 (1969)
[27] J. D. Bjorken and E. A. Paschos, Phys. Rev. **185**, 1975 (1969)
[28] R. D. Ball, V. Bertone, F. Cerutti, L. Del Debbio, S. Forte, A. Guffanti, J. I. Latorre, J. Rojo, and M. Ubiali (NNPDF), Nucl. Phys. B **855**, 153 (2012), arXiv: 1107.2652[hep-ph]
[29] J. Pumplin, D. R. Stump, J. Huston, H. L. Lai, P. M. Nadolsky, and W. K. Tung, JHEP **07**, 012 (2002), arXiv: hep-ph/0201195
[30] S. Dulat, T.-J. Hou, J. Gao, M. Guzzi, J. Huston, P. Nadolsky, J. Pumplin, C. Schmidt, D. Stump, and C. P. Yuan, Phys. Rev. D **93**, 033006 (2016), arXiv: 1506.07443[hep-ph]
[31] R. Wang and X. Chen, Chin. Phys. C **41**, 053103 (2017), arXiv: 1609.01831[hep-ph]
[32] R. Wang, C. Han, and X. Chen, Phys. Rev. D **110**, 114011 (2024), arXiv: 2407.16122[hep-ph]
[33] P.-L. Yin, Y.-Z. Xu, Z.-F. Cui, C. D. Roberts, and J. Rodríguez-Quintero, Chin. Phys. Lett. **40**, 091201 (2023), arXiv: 2306.03274[hep-ph]
[34] R. Wang and X. Chen, Phys. Rev. D **91**, 054026 (2015), arXiv: 1410.3598[hep-ph]
[35] J. C. Collins and D. E. Soper, Ann. Rev. Nucl. Part. Sci. **37**, 383 (1987)
[36] J. C. Collins, D. E. Soper, and G. F. Sterman, Adv. Ser. Direct. High Energy Phys. **5**, 1 (1989), arXiv: hep-ph/0409313
[37] G. F. Sterman, in *Theoretical Advanced Study Institute in Elementary Particle Physics (TASI 95): QCD and Beyond* (1995) pp. 327–408, arXiv: hep-ph/9606312
[38] G. Altarelli, N. Cabibbo, L. Maiani, and R. Petronzio, Nucl. Phys. B **69**, 531 (1974)
[39] G. Parisi and R. Petronzio, Phys. Lett. B **62**, 331 (1976)
[40] M. Gluck and E. Reya, Nucl. Phys. B **130**, 76 (1977)
[41] R. L. Jaffe and G. G. Ross, Phys. Lett. B **93**, 313 (1980)
[42] M. Gluck, E. Reya, and A. Vogt, Z. Phys. C **48**, 471 (1990)
[43] M. Gluck, E. Reya, and A. Vogt, Z. Phys. C **53**, 127 (1992)
[44] M. Gluck, E. Reya, and A. Vogt, Z. Phys. C **67**, 433 (1995)
[45] M. Traini, A. Mair, A. Zambarda, and V. Vento, Nucl. Phys. A **614**, 472 (1997)
[46] S. Scopetta, V. Vento, and M. Traini, Phys. Lett. B **421**, 64 (1998), arXiv: hep-ph/9708262
[47] S. Scopetta and V. Vento, Eur. Phys. J. A **16**, 527 (2003), arXiv: hep-ph/0201265
[48] E. Ruiz Arriola, Nucl. Phys. A **641**, 461 (1998)
[49] Y. L. Dokshitzer, Sov. Phys. JETP **46**, 641 (1977)
[50] V. N. Gribov and L. N. Lipatov, Sov. J. Nucl. Phys. **15**, 438 (1972)
[51] G. Altarelli and G. Parisi, Nucl. Phys. B **126**, 298 (1977)
[52] M. Diehl and P. Stienemeier, Eur. Phys. J. Plus **135**, 211 (2020), arXiv: 1904.10722[hep-ph]
[53] R. G. Roberts, Eur. Phys. J. C **10**, 697 (1999), arXiv: hep-ph/9904317
[54] A. Courtoy and S. Liuti, Int. J. Mod. Phys. Conf. Ser. **20**, 266 (2012), arXiv: 1208.5636[hep-ph]
[55] A. C. Aguilar, D. Binosi, J. Papavassiliou, and J. Rodriguez-Quintero, Phys. Rev. D **80**, 085018 (2009), arXiv: 0906.2633[hep-ph]
[56] C. S. Armstrong, R. Ent, C. E. Keppel, S. Liuti, G. Niculescu, and I. Niculescu, Phys. Rev. D **63**, 094008 (2001), arXiv: hep-ph/0104055
[57] K. D. Lane, Phys. Rev. D **10**, 2605 (1974)
[58] H. D. Politzer, Nucl. Phys. B **117**, 397 (1976)
[59] J. M. Cornwall and J. Papavassiliou, Phys. Rev. D **40**, 3474 (1989)
[60] Y. Nambu and G. Jona-Lasinio, Phys. Rev. **122**, 345 (1961)
[61] G. Krein, C. D. Roberts, and A. G. Williams, Int. J. Mod. Phys. A **7**, 5607 (1992)
[62] L. Chang, C. D. Roberts, and D. J. Wilson, PoS **QCD-TNT-II 2011**, 039 (2011), arXiv: 1201.3918[nucl-th]
[63] C. D. Roberts, Prog. Part. Nucl. Phys. **61**, 50 (2008), arXiv: 0712.0633[nucl-th]
[64] H. J. Munczek, Phys. Rev. D **52**, 4736 (1995), arXiv: hep-th/9411239
[65] D. Binosi, C. Mezrag, J. Papavassiliou, C. D. Roberts, and J. Rodriguez-Quintero, Phys. Rev. D **96**, 054026 (2017), arXiv: 1612.04835[nucl-th]
[66] Z.-F. Cui, J.-L. Zhang, D. Binosi, F. de Soto, C. Mezrag, J. Papavassiliou, C. D. Roberts, J. Rodríguez-Quintero, J. Segovia, and S. Zafeiropoulos, Chin. Phys. C **44**, 083102 (2020a), arXiv: 1912.08232[hep-ph]
[67] Y. Yu, P. Cheng, H.-Y. Xing, F. Gao, and C. D. Roberts, Eur. Phys. J. C **84**, 739 (2024), arXiv: 2402.06095[hep-ph]
[68] Y. Lu, L. Chang, K. Raya, C. D. Roberts, and J. Rodríguez-Quintero, Phys. Lett. B **830**, 137130 (2022), arXiv: 2203.00753[hep-ph]
[69] L. Chang, C. Mezrag, H. Moutarde, C. D. Roberts, J. Rodríguez-Quintero, and P. C. Tandy, Phys. Lett. B **737**, 23 (2014), arXiv: 1406.5450[nucl-th]
[70] M. Ding, K. Raya, D. Binosi, L. Chang, C. D. Roberts, and S. M. Schmidt, Phys. Rev. D **101**, 054014 (2020), arXiv:


CPC Accepted

1905.05208[nucl-th]
[71] Z.-F. Cui, M. Ding, F. Gao, K. Raya, D. Binosi, L. Chang, C. D. Roberts, J. Rodríguez-Quintero, and S. M. Schmidt, Eur. Phys. J. C **80**, 1064 (2020b)
[72] X. Ji, Phys. Rev. Lett. **110**, 262002 (2013), arXiv: 1305.1539[hep-ph]
[73] X. Ji, Sci. China Phys. Mech. Astron. **57**, 1407 (2014), arXiv: 1404.6680[hep-ph]
[74] X. Ji, Y.-S. Liu, Y. Liu, J.-H. Zhang, and Y. Zhao, Rev. Mod. Phys. **93**, 035005 (2021), arXiv: 2004.03543[hep-ph]
[75] X. Ji, J.-H. Zhang, and Y. Zhao, Phys. Rev. Lett. **120**, 112001 (2018), arXiv: 1706.08962[hep-ph]
[76] Y.-Q. Ma and J.-W. Qiu, Phys. Rev. D **98**, 074021 (2018a), arXiv: 1404.6860[hep-ph]
[77] Y.-Q. Ma and J.-W. Qiu, Phys. Rev. Lett. **120**, 022003 (2018b), arXiv: 1709.03018[hep-ph]
[78] J. Lan, C. Mondal, S. Jia, X. Zhao, and J. P. Vary, Phys. Rev. D **101**, 034024 (2020), arXiv: 1907.01509[nucl-th]
[79] C. Mondal, S. Xu, J. Lan, X. Zhao, Y. Li, D. Chakrabarti, and J. P. Vary, Phys. Rev. D **102**, 016008 (2020), arXiv: 1911.10913[hep-ph]
[80] R. J. Holt and C. D. Roberts, Rev. Mod. Phys. **82**, 2991 (2010), arXiv: 1002.4666[nucl-th]
[81] H. Mineo, W. Bentz, N. Ishii, A. W. Thomas, and K. Yazaki, Nucl. Phys. A **735**, 482 (2004), arXiv: nucl-th/0312097
[82] A. Kock, Y. Liu, and I. Zahed, Phys. Rev. D **102**, 014039 (2020), arXiv: 2004.01595[hep-ph]
[83] F. M. Steffens and A. W. Thomas, Prog. Theor. Phys. Suppl. **120**, 145 (1995), arXiv: hep-ph/9509244
[84] A. Radyushkin, Annalen Phys. **13**, 718 (2004), arXiv: hep-ph/0410153
[85] A. C. Aguilar, F. De Soto, M. N. Ferreira, J. Papavassiliou, J. Rodríguez-Quintero, and S. Zafeiropoulos, Eur. Phys. J. C **80**, 154 (2020), arXiv: 1912.12086[hep-ph]
[86] A. Bender, C. D. Roberts, and L. Von Smekal, Phys. Lett. B **380**, 7 (1996), arXiv: nucl-th/9602012
[87] W. Zhu and F. Wang, (2019), arXiv: 1912.09785[hep-ph]
[88] L. V. Gribov, E. M. Levin, and M. G. Ryskin, Phys. Rept. **100**, 1 (1983)
[89] A. H. Mueller and J.-w. Qiu, Nucl. Phys. B **268**, 427 (1986)
[90] W. Zhu, Nucl. Phys. B **551**, 245 (1999), arXiv: hep-ph/9809391
[91] W. Zhu, R. Wang, J. Ruan, X. Chen, and P. Zhang, Eur. Phys. J. Plus **131**, 6 (2016), arXiv: 1404.0759[hep-ph]
[92] X. Chen, J. Ruan, R. Wang, P. Zhang, and W. Zhu, Int. J. Mod. Phys. E **23**, 1450057 (2014), arXiv: 1306.1872[hep-ph]
[93] O. Nachtmann, Nucl. Phys. B **63**, 237 (1973)
[94] I. Schienbein *et al.*, J. Phys. G **35**, 053101 (2008), arXiv: 0709.1775[hep-ph]
[95] P. C. Barry, C.-R. Ji, N. Sato, and W. Melnitchouk (Jefferson Lab Angular Momentum (JAM)), Phys. Rev. Lett. **127**, 232001 (2021), arXiv: 2108.05822[hep-ph]
[96] G. Corcella and L. Magnea, Phys. Rev. D **72**, 074017 (2005), arXiv: hep-ph/0506278
[97] M. Bonvini, S. Marzani, J. Rojo, L. Rottoli, M. Ubiali, R. D. Ball, V. Bertone, S. Carrazza, and N. P. Hartland, JHEP **09**, 191 (2015), arXiv: 1507.01006[hep-ph]
[98] M. Aicher, A. Schafer, and W. Vogelsang, Phys. Rev. Lett. **105**, 252003 (2010), arXiv: 1009.2481[hep-ph]
[99] D. Westmark and J. F. Owens, Phys. Rev. D **95**, 056024 (2017), arXiv: 1701.06716[hep-ph]
[100] I. Niculescu, C. Keppel, S. Liuti, and G. Niculescu, Phys. Rev. D **60**, 094001 (1999)
[101] J.-X. Yu, S. Cheng, J.-J. Han, H.-n. Li, and F.-S. Yu, Eur. Phys. J. C **86**, 300 (2026), arXiv: 2511.12589[hep-ph]
[102] W. Melnitchouk, R. Ent, and C. Keppel, Phys. Rept. **406**, 127 (2005), arXiv: hep-ph/0501217
[103] W. G. Seligman *et al.* (CCFR), Phys. Rev. Lett. **79**, 1213 (1997), arXiv: hep-ex/9701017
[104] M. Tzanov *et al.* (NuTeV), Phys. Rev. D **74**, 012008 (2006), arXiv: hep-ex/0509010
[105] A. Deur, V. Burkert, J. P. Chen, and W. Korsch, Particles **5**, 171 (2022), arXiv: 2205.01169[hep-ph]

CPC Accepted